Chinese Chemical Letters 37 (2026) 111585

Contents lists available at ScienceDirect

Chinese Chemical Letters

journal homepage: www.elsevier.com/locate/cclet

Arsenic trioxide-induced pyroptosis promotes the release of HMGB1 to activate natural killer cells related immunogenic cell death in leukemia

Jia-Yin Su[a,d,1], Shiyao Song[a,1], Zi-Min Song[b], Xi Sun[c], Niangji Tsomo[e], Ying-Li Liu[f], Jingxuan Ma[g], Jie-Si Luo[a], Li-Na Wang[a], Suoyu Xiang[c], Cong Liang[a], Xue-Qun Luo[a], Jun Wu[h,i,*], Li-Bin Huang[a,*], Yan-Lai Tang[a,*]

[a] Department of Paediatrics, the First Affiliated Hospital, Sun Yat-sen University, Guangzhou 510080, China
[b] Center of Hepato-Pancreato-Biliary Surgery, the First Affiliated Hospital, Sun Yat-sen University, Guangzhou 510080, China
[c] Department of Parasitology of Zhongshan School of Medicine, Sun Yat-sen University, Guangzhou 510080, China
[d] School of Life Science, The Chinese University of Hong Kong, Hong Kong SAR 999077, China
[e] Research Center for High Altitude Medicine, School of Medicine, Qinghai University, Xining 810000, China
[f] Shenzhen Longgang Otorhinolaryngology Hospital, Shenzhen 518100, China
[g] West China School of Medicine, Sichuan University, Chengdu 610044, China
[h] Division of Life Science, The Hong Kong University of Science and Technology, Hong Kong SAR 999077, China
[i] Bioscience and Biomedical Engineering Thrust, The Hong Kong University of Science and Technology (Guangzhou), Guangzhou 511400, China

ARTICLE INFO

Article history:
Received 16 April 2025
Revised 11 July 2025
Accepted 13 July 2025
Available online 14 July 2025

Keywords:
Arsenic trioxide
Pyroptosis
Natural killer cells
Acute myeloid leukemia
Immunogenic cell death

ABSTRACT

The application of Arsenic trioxide (ATO) has greatly improved the cure rates in patients with acute promyelocytic leukemia (APL) and has shown therapeutic effects in other leukemia types, as evidenced by an increasing number of preclinical trials. However, its clinical application is still limited due to a lack of understanding of the underlying mechanisms. In this report, we have demonstrated that ATO can induce pyroptosis and release damage-associated molecular patterns (DAMPs), such as high mobility group box 1 (HMGB1) and interleukin-1β (IL-1β). DAMPs can activate the immunogenic cell death (ICD) mechanism. Our study elucidated the pivotal role of pyroptosis and demonstrated the activation of the caspase-3/gasdermin E (GSDME) pathway both *in vivo* and *in vitro* upon ATO intervention. Proteomic analysis of cell supernatants revealed the release of the ICD-associated molecule HMGB1. Results from both *in vitro* and *in vivo* experiments collectively demonstrated that the release of HMGB1 is contingent upon GSDME-mediated pyroptosis. Furthermore, label-free quantitative proteomics *in vivo* indicated that ATO-induced pyroptosis activates natural killer cells (NKs) and promotes the release of granzyme B (GZMB). Our study is the first to demonstrate the synergistic interplay between pyroptosis and ICD mechanisms during ATO treatment, providing novel insights into the potential of ATO for immunotherapy and synergistic treatment approaches.

© 2026 Published by Elsevier B.V. on behalf of Chinese Chemical Society and Institute of Materia Medica, Chinese Academy of Medical Sciences.

Arsenic trioxide (ATO), mainly applied in the chemotherapy in acute promyelocytic leukemia (APL) [1]. The remarkable efficacy of ATO combined with all-*trans* retinoic acid (ATRA) in the treatment of APL has increased the cure rate to 80%–90%, drawing widespread attention from the global scientific community [2]. Previous research has demonstrated that ATO is effective in treating a range of leukemias [3–5]. Moreover, studies have shown that ATO exhibits broad-spectrum anticancer effects against hepatocellular carcinoma, glioblastoma, and other malignancies [6–8]. However, the outcomes of most clinical trials do not exhibit the same efficacy as observed in preclinical models [9]. Therefore, a more comprehensive understanding of the tumor treatment mechanisms of ATO is essential to elucidate its clinical limitations and to develop novel combination therapies and application strategies to benefit patients.

Pyroptosis is a form of regulated cell death (RCD) mediated by inflammatory pathways [10,11]. Pyroptosis not only causes membrane rupture but also induces the maturation of caspase-1 and the release of substantial amounts of inflammatory cytokines, par-

* Corresponding authors.
E-mail addresses: junwuhkust@ust.hk (J. Wu), huanglb3@mail.sysu.edu.cn (L.-B. Huang), tangylai@mail.sysu.edu.cn (Y.-L. Tang).
[1] These authors contributed equally to this work.

https://doi.org/10.1016/j.cclet.2025.111585
1001-8417/© 2026 Published by Elsevier B.V. on behalf of Chinese Chemical Society and Institute of Materia Medica, Chinese Academy of Medical Sciences.

ticularly pro-inflammatory cytokines such as interleukin-1β (IL-1β) and IL-18, which can elicit a robust immune response both locally and systemically [12]. The hallmark of pyroptosis is the cleavage and activation of gasdermin proteins, such as gasdermin E (GSDME) and GSDMD. Caspases cleave gasdermins at their central linker, releasing autoinhibition from the gasdermin-N fragment, which dictates its pore-forming activity, essential to the process of pyroptosis. One research has shown that some compounds, such as polycyclic polyprenylated acylphloroglucinols (PPAPs), can promote endogenous inflammation and cell death in acute myeloid leukemia (AML) cells [13,14]. Previous studies have also demonstrated that arsenic exposure induces pyroptosis in the liver [15]. However, it remains unclear whether the same pyroptosis mechanism occurs during arsenic treatment of tumors.

Immunogenic cell death (ICD) is another form of RCD that not only leads to the demise of tumor cells but also releases a series of molecules known as damage-associated molecular patterns (DAMPs) [16]. These DAMPs, such as high mobility group box 1 (HMGB1), can activate immune cells, such as natural killer cells (NKs), thereby initiating a specific immune response [17–19]. Furthermore, a mutually reinforcing relationship exists between pyroptosis and NKs. During pyroptosis, the formation of pores in the cell membrane leads to the release of DAMPs [20]. Immunoproteins, such as HMGB1, can participate in lymphocyte differentiation and regulate the activation of NKs [21,22]. On the other hand, NKs degranulation release granzyme, which can directly induce caspase-independent pyroptosis [23,24]. ATO has previously been shown to enhance the cytotoxicity of NKs [25]. However, it remains unclear whether pyroptosis is involved in the occurrence of ICD induced by ATO.

Therefore, our study aimed to explore the association between ATO treatment, pyroptosis induction, and its effect on ICD in AML. Our study found that ATO induced pyroptosis primarily through the GSDME pathway, and HMGB1 release was detected *via* supernatant proteomics. Additionally, proteomic analysis *in vivo* model revealed abnormal ICD activation, and we confirmed that this mechanism was driven by the activation of NKs. Moreover, this activation mechanism is dependent on GSDME-mediated pyroptosis. In summary, we found that ATO induces GSDME-mediated pyroptosis, followed by activation of the NKs-dominated ICD mechanism. These findings offer a deeper understanding of the therapeutic mechanisms of ATO and suggest potential avenues for subsequent combination therapies.

To explore the biological functions of pyroptosis in AML, 468 AML patient samples from three databases, TARGET (https://ocg.cancer.gov/programs/target), TCGA (https://portal.gdc.cancer.gov/), and GEO (https://www.ncbi.nlm.nih.gov/), were analyzed to compare the prognostic outcomes of the GSDMD high and low groups. As a crucial protein in the pyroptosis pathway, the GSDMD high and low groups represent high or low expression levels of pyroptosis-related genes (PRGs). As shown in Fig. S1 (Supporting information), all three datasets revealed a significant prognostic difference between high and low expressions of PRGs (Figs. S1A–C). These results indicate that pyroptosis is closely related to the development and treatment of AML.

Subsequently, we explored the relationship between ATO and pyroptosis in clinical treatment. With the consent of the patient or the patient's family, we extracted the patient's primary cells and performed ATO drug sensitivity tests and next-generation sequencing (Fig. S1D). We classified 11 patients into hypersensitive and hyposensitive groups, using a cyto-inhibition rate of 50% as the threshold (Fig. S1E). Next, 33 PRGs were extracted from the sequencing results of patient cells, and we analyzed the differences between the hypersensitive and hyposensitive groups. The results showed that GSDMA, caspase-5 (CASP5), NOD-like receptor protein 3 (NLRP3), IL1B, and GSDME were upregulated in the hyposensitive group, while GSDMB, CASP3, and nucleotide-binding oligomerization domain containing 1 (NOD1) were downregulated (Fig. S1F). These results were corroborated by the analysis of differences between AML patient samples from TCGA and TARGET databases and normal samples from GTEx database (https://www.gtexportal.org) (Figs. S1A and B). Thus, the expression of PRGs significantly affects the efficacy of ATO treatment.

AML cell lines (MV411 and MOLM13) were treated with gradient doses (0, 1.5, 3, and 6 μmol/L) of ATO for 24 h in the ATO group and with DMSO in the negative control (NC) group. Microscopic observations revealed that AML cells treated with ATO exhibited typical pyroptotic morphology, characterized by large bubbles (indicated by red arrows) emerging from the plasma membrane and cell swelling, which were not observed in the absence of ATO treatment. The ratio of pyroptotic cells increased in correlation with the ATO dosage (Fig. 1A and Fig S5D in Supporting information). Flow cytometry analyses indicated that the percentage of propidium iodide (PI)-positive cells increased in accordance with the ATO dosage ($P < 0.05$) (Fig. S5A in Supporting information). The cytotoxicity lactate dehydrogenase (LDH) assay results demonstrated a significant increase in LDH release activity in AML cells treated with ATO, which was dose-dependent (Fig. 1C). To elucidate the mechanism associated with ATO-induced pyroptosis, we assessed the relative gene expression levels of GSDMD and GSDME using real-time quantitative PCR (RT-qPCR). Our findings indicated that GSDME expression levels increased in a dose-dependent manner with ATO, while GSDMD did not (Figs. S5B and C in Supporting information). Consequently, we conducted a Western blot (WB) assay to evaluate the activation of the caspase-3/GSDME pyroptotic pathway, finding that the protein expression levels of the N-terminal of GSDME (GSDME-N) and cleaved-caspase-3 significantly increased in a dose-dependent manner with ATO (Fig. 1B and Fig S5F in Supporting information). Additionally, we investigated two classical inflammatory factors associated with pyroptosis, IL-18 and IL-1β, released in response to ATO treatment, utilizing enzyme-linked immunoorbent assay (ELISA) assays. The results demonstrated that the release of IL-1β in the cell culture supernatant was dose-dependently enhanced with increasing doses of ATO treatment (Fig. 1D). In contrast, the release of IL-18 was not enhanced in both AML cell lines (Fig. 1E).

To further verify that ATO-induced pyroptosis occurs *via* the caspase-3/GSDME pathway, we administered Z-DEVD-FMK (a caspase-3 inhibitor) at a concentration of 25 μmol/L in the ATO+DEVD group. WB results indicated that as the protein level of caspase-3 was inhibited, the protein level of GSDME-N was significantly down-regulated (Fig. 1G and Fig S5G in Supporting information). Fig. 1F demonstrated a decreased ratio of pyroptotic cells (indicated by red arrows) and an increased ratio of apoptotic cells (indicated by white arrows) in the ATO+DEVD group. Flow cytometry analysis also revealed a decreased ratio of PI-positive cells in the ATO+DEVD group (Figs. S6A–C in Supporting information). The results of the cytotoxicity LDH assay demonstrated that LDH release from AML cells significantly decreased in the ATO+DEVD group (Fig. 1H). Furthermore, compared to the ATO group, the ATO+DEVD group exhibited a significantly reduced level of IL-1β and IL-18 (Figs. 1I and J). These results indicate that ATO treatment induces pyroptosis in a dose-dependent manner, characterized by LDH release and activation of the caspase-3/GSDME pathway.

To further investigate the effects of ATO-induced pyroptosis on the extracellular environment, as shown in Fig. S2 (Supporting information), we collected supernatants from AML cells in both NC and ATO groups for electrophoretic and proteomic analysis (Fig. S2A). The electrophoretic analysis revealed specific protein bands in the ATO group. Mass spectrometry analysis identified 1600 proteins in supernatants treated with ATO, compared to 1365 in the NC group (Fig. S2B). Additionally, mass spectrometry analysis also

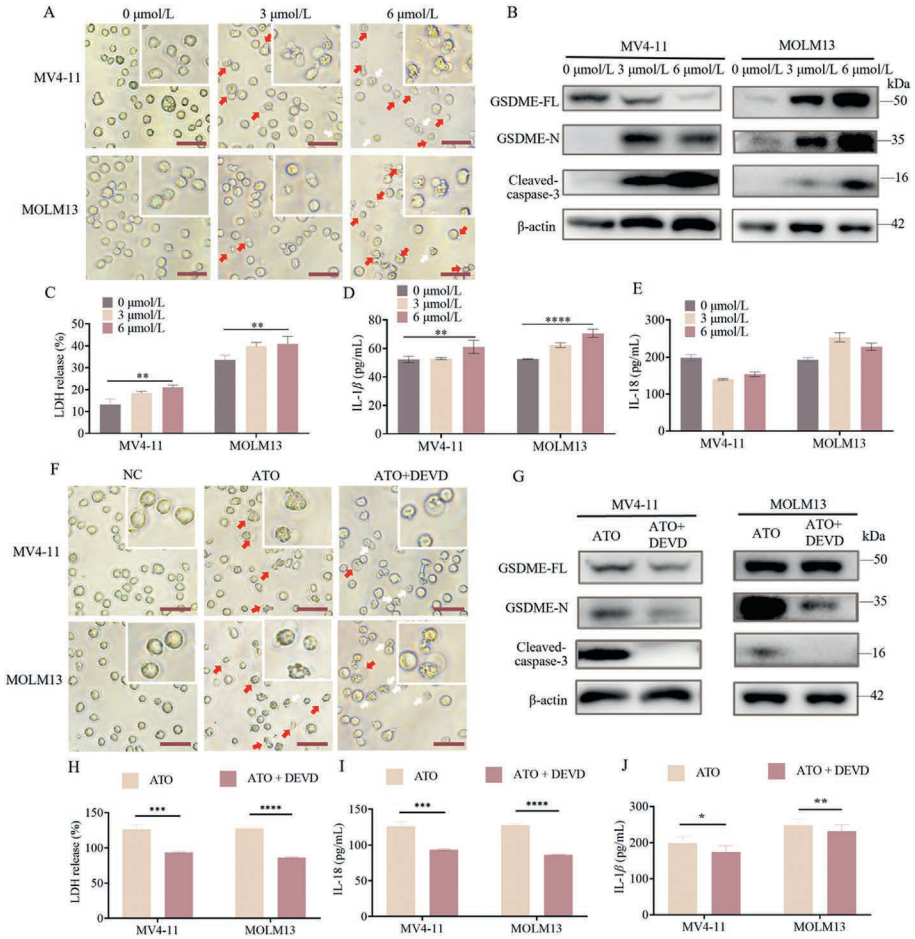


Fig. 1. ATO induced pyroptosis in AML cells *via* the activation of caspase-3/GSDME pathway. (A) Representative microscopic images of AML cells after ATO treatment for 24 h (400×). The red arrows denote the typical balloon in the membrane of pyroptosis cells. Scale bar: 20 μm. (B) The expression levels of GSDME-FL, the GSDME-N, and cleaved-caspase-3 were detected by WB in AML cells. (C) The release of LDH of AML cells was measured by cytotoxicity LDH assay. (D, E) The release levels of IL-1β and IL-18 were detected by ELISA in the supernatants of AML cells. (F) Representative microscopic images of AML cells in ATO and ATO+DEVD groups (400×). Scale bar: 20 μm. (G) The expression levels of GSDME-FL, GSDME-N, and cleaved-caspase-3 were detected by WB after ATO or ATO+DEVD treatment. (H) The release of LDH of AML cells was measured by cytotoxicity LDH assay. (I, J) The release levels of IL-18 and IL-1β were detected by ELISA in the supernatants of AML cells in ATO and ATO+DEVD groups. All the data is presented as mean ± SD from at least 3 independent experiments. ns: not significant. $^{*}P < 0.05$, $^{**}P < 0.01$, $^{***}P < 0.001$, $^{****}P < 0.0001$ using one-way ANOVA.

showed a tenfold or greater increase in 78 proteins in the ATO group compared to the NC group (listed in Table S3 in Supporting information). We further conducted enrichment analysis on the significantly altered genes. The results indicated multiple factors closely related to the immune system (Fig. S7 in Supporting information), with 78 proteins, including HMGB1, involved in immune responses (Fig. S2C).

Next, we then assessed HMGB1 release capacity in the different groups. HMGB1 levels in the extracellular environment were quantified using ELISA. The results showed that HMGB1 content increased with ATO dosage, which could be inhibited by Z-DEVD-FMK (Fig. S2D). We also performed immunofluorescence analysis to verify the difference in HMGB1 distribution between the NC and ATO groups. The results showed that HMGB1 in the ATO group was more prominently distributed in the cytoplasm compared to the NC group (Fig. S2E). These results suggest that ATO-induced pyroptosis enhances the release of HMGB1, potentially regulating the process of ICD to further promote AML cell elimination.

To verify the induction of pyroptosis by ATO and the activation of the caspase-3/GSDME pathway, we conducted animal experiments with nude mice, which were complied with international and national animal welfare guidelines. The *in vivo* assay using nude mice were approved by the Institutional Animal Care and Use Committee of The First Affiliated Hospital of Sun Yat-sen University (No. [2021] 040). We followed the 3R (replacement, reduction, refinement) principles, and proper anesthesia or analgesia was used to minimize animal discomfort. Mice were transplanted with MV4–11 cells to develop AML xenograft tumors, which were then divided into two groups: ATO-treated and phosphate balanced solution (PBS)-treated as control (Fig. 2A). Images of dissected AML xenograft tumors revealed a reduction in tumor size in the ATO-treated group (Fig. 2B). Consistently, the tumor growth curve demonstrated a significantly slower increase in tumor volume in the ATO-treated group compared to the control group (Fig. 2C). Ki-67 (Nuclear Proliferation-Associated Antigen) staining results revealed lower expression of Ki-67 in the ATO-treated group compared to the NC group, indicating a suppression of tumor proliferation (Fig. 2D). Hematoxylin and eosin (HE) staining further indicated an expansion of tumor necrosis in the ATO-treated group (Fig. S8A in Supporting information). To assess the potential side effects of ATO treatment, body weight, liver weight, and spleen weight were measured, and liver tissues were examined *via* HE staining. The results showed no significant differences between the ATO-treated and control groups (Figs. S8C–E in Supporting information).

Additionally, we examined the expression of pyroptosis-related proteins and HMGB1 released. WB analysis revealed significantly increased expression of full-length GSDME (GSDME-FL), GSDME-N,

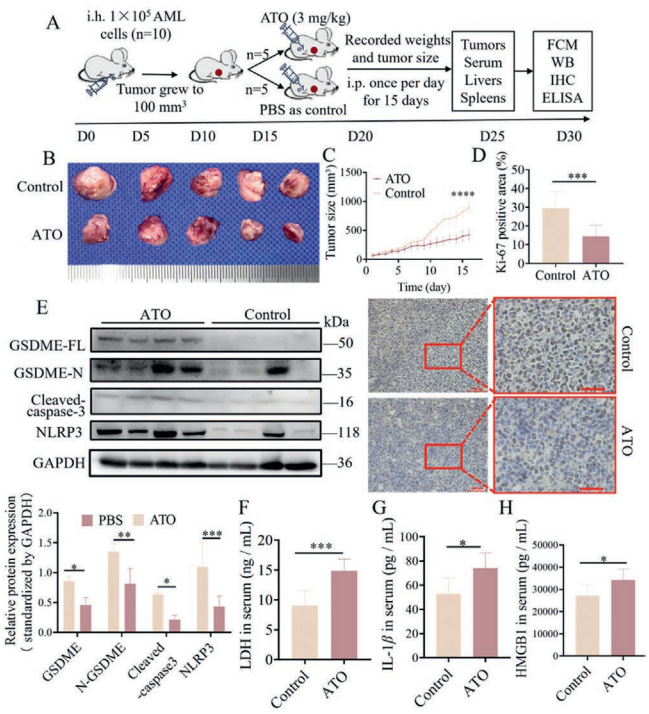


Fig. 2. ATO activated caspase-3/GSDME pyroptotic pathway and enhanced the release of HMGB1 and cytokines IL-1β *in vivo*. ATO (3 mg/kg) was injected intraperitoneally into AML xenograft mice ($n = 5$) in the ATO group and the same volume of PBS was injected in the control group for 15 days. (A) Schematic representation of the establishment and drug treatment of AML xenograft nude mice in the ATO group and the control group. (B) The images of dissected tumors of AML xenograft mice in two groups (C) The average tumor volume (mm^3) curve of the two groups was measured every day in the period of drug treatment. (D) Quantitative analysis of the immunohistochemical staining of Ki-67. Scale bar: 100 μm (left) and 40 μm (right). (E) The relative protein expression levels of GSDME-FL, GSDME-N, cleaved-caspase-3, and NLRP3 were detected by WB in AML xenograft tumor of the two groups. (F-H) The release levels of LDH, HMGB1 and IL-1β in the serum of AML xenograft mice in the two groups were measured by ELISA. The data were presented as mean ± SEM. $^{*}P < 0.05$, $^{**}P < 0.01$, $^{***}P < 0.001$. GAPDH, glyceraldehyde-3-Phosphatedehydrogenase.

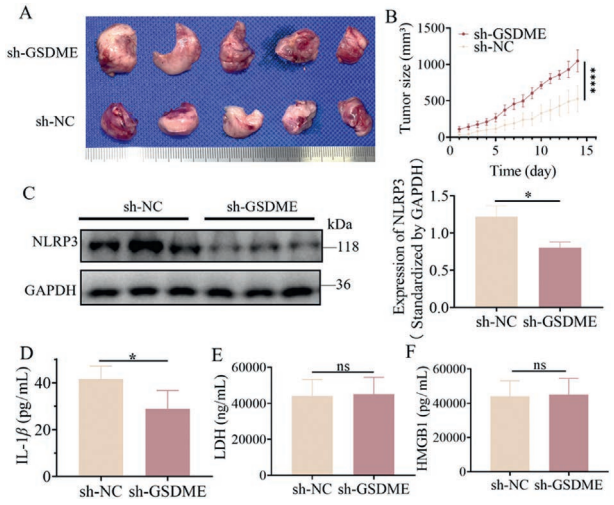


Fig. 3. GSDME knockdown rescue tumor inhibition and inhibit IL1β release through NLRP3. (A) The images the dissected tumors of AML xenograft mice in two groups after 3 mg/kg ATO treatment daily for 15 days. (B) The average tumor volume (mm^3) curve of the two groups was measured every day in the period of drug treatment (presented as mean ± SD). (C) The relative protein expression levels of NLRP3 were detected by WB in AML xenograft tumor. (D–F) The release levels of IL-1β, LDH, and HMGB1 in the serum of AML xenograft mice were measured by ELISA. $^{*}P < 0.05$ using *t*-test.

and cleaved-caspase-3 in the AML xenograft tumors of the ATO-treated group (Fig. 2E), confirming the activation of the caspase-3/GSDME pyroptotic pathway. Furthermore, we observed an increase in NLRP3 protein expression in the GSDME-high expression group, suggesting a positive correlation between NLRP3 and GSDME-N expression. Additionally, we assessed the serum levels of DAMPs and proinflammatory cytokines using ELISA, and the results indicated significantly increased secretion of LDH, HMGB1, and IL-1β in the ATO-treated group (Figs. 2F–H).

To further investigate the involvement of the caspase-3/GSDME pathway in ATO-induced pyroptosis, MV4–11 cells, with stable GSDME knockdown *via* small hairpin RNA (shRNA) packaged lentivirus, were transplanted into nude mice to develop sh-GSDME AML xenograft tumors in mice. When tumors reached approximately 100 mm^3, AML xenograft mice were treated with 3 mg/kg ATO intraperitoneally once daily. After 15 days, serum and tumor samples were collected. The effectiveness of GSDME knockdown was validated by WB analysis both *in vivo* and *in vitro* (Fig. S9 in Supporting information). Images of dissected AML xenograft tumors and the tumor growth curve demonstrated significantly increased tumor size and progression rate in the sh-GSDME group, indicating that GSDME knockdown accelerated AML tumor progression *in vivo* (Figs. 3A and B). Consistent with previous findings, the GSDME pathway plays a key role in ATO-induced pyroptosis.

GSDME-N is known to stimulate the expression of NLRP3 [26]. To further investigate whether NLRP3 was activated by GSDME-N in our AML xenograft models, we examined NLRP3 expression in the sh-GSDME and sh-NC groups and found that GSDME knockdown significantly inhibited NLRP3 activation (Fig. 3C). Furthermore, we assessed serum levels of LDH, HMGB1, and IL-1β by ELISA. The results revealed that IL-1β secretion was significantly lower in the sh-GSDME group compared to the sh-NC group, indicating that GSDME knockdown significantly suppressed ATO-induced IL-1β upregulation (Fig. 3D). However, no significant differences in LDH or HMGB1 release were observed between the two groups (Figs. 3E and F). The downstream molecule NLRP3 is significantly downregulated, leading to the mature IL-1β reduced. Collectively, these data suggest that ATO activates the caspase-3/GSDME pathway to induce pyroptosis, and GSDME upregulates NLRP3 expression, which in turn enhances IL-1β release and inhibits tumor progression in AML xenograft mice.

To further elucidate the underlying mechanisms and functional systems involved in the anti-tumor effect of ATO, as shown in Fig. S3 (Supporting information), we employed label-free quantitative proteomics to analyze the differentially expressed proteins (DEPs) in AML xenograft tumors from the ATO and control (PBS) groups (Fig. S3A). A total of 4618 proteins were identified through quantitative proteomic analysis. Based on the criteria of a fold change greater than 1.5 and *P*-value < 0.05, we identified 63 upregulated and 20 downregulated proteins in the ATO group compared to the PBS group (Table S5 in Supporting information). The DEPs are presented as a volcano plot (Fig. S3B). This finding is consistent with the *in vitro* proteomic results. Kyoto encyclopedia of genes and genomes pathway (KEGG) pathway analysis revealed that the immune system exhibited the highest number of DEPs (Fig. S3C). KEGG pathway analysis further shows that the upregulated DEPs are predominantly enriched in the mitogen-activated protein kinases (MAPK) cell death signaling pathway, NOD-like receptor signaling pathway, and Th17 cell differentiation (Figs. S3D and E). Notably, the MAPK cell death signaling pathway and NOD-like receptor signaling pathway were the most significantly altered. The targets of these pathways included cathepsin B (CTSB), mitogen-

activated protein kinase 14 (p38), p53, and NLRP3, which were subsequently validated by WB analysis (Fig. 3D and Fig. S3F).

As suggested by the proteomic results, the immune system has been activated. We hypothesized that pyroptosis induced by ATO could enhance the immune cell death (ICD) activity of NKs. Therefore, we compared NKs recruitment and GZMB degranulation between the ATO and NC groups. To validate the involvement of GSDME-mediated pyroptosis in the activation of NKs by ATO, we transplanted MV4–11 cells with stable knockdown of endogenous GSDME *via* shRNA-expressing lentivirus into nude mice in the sh-GSDME group to establish AML models with reduced GSDME expression. MV4–11 cells infected with control shRNA lentivirus were transplanted into the sh-NC group as a control. Flow cytometry analysis of NKs (CD16+CD49b+) demonstrated that the percentage of NKs was significantly increased in the tumors, peripheral blood, and spleen of mice in the ATO group compared to the control group (Fig. 4A). Furthermore, the percentage of NKs was reduced in the sh-GSDME group compared to the sh-NC group (Fig. 4B), suggesting that ATO upregulated the recruitment and tumor infiltration capacity of NKs, a process dependent on GSDME.

Additionally, the expression and release of GZMB were evaluated. Immunofluorescence staining results indicated that the expression levels of GZMB were upregulated in tumor-infiltrating NKs in the ATO group (Figs. 4C and D). WB analysis further revealed that the expression level of GZMB in the ATO group was higher than that in the control group (Fig. S12 in Supporting information). Additionally, the GZMB release level in the serum of the ATO group was significantly higher compared to the control group (Fig. 4E). And the release level in the sh-GSDME group tended to decrease compared to the sh-NC group (Fig. 4F). This suggests that ATO stimulated GZMB granulation in NKs *in vivo*, a process mediated by the GSDME pathway.

Next, we conducted co-culture experiments to investigate the crosstalk between pyroptosis and ICD induced by ATO. MV4–11 cells were pretreated with ATO (0, 3, 6 μmol/L), washed with PBS to remove residual drug, and then co-cultured with NK92-MI cells (Fig. 4G). Cell counting kit-8 (CCK-8) assay results demonstrated that the proliferation of NK-92MIs co-cultured with MV4–11 cells pretreated with ATO was significantly upregulated compared to those co-cultured with MV4–11 cells without ATO pretreatment (Fig. 4H). ELISA results revealed that GZMB release from NK-92MIs co-cultured with MV4–11 cells pretreated with ATO was significantly increased in a dose-dependent manner compared to those co-cultured with MV4–11 cells without ATO pretreatment (Fig. 4I). This increase was inhibited by Z-DEVD-FMK (caspase-3 specific inhibitor) (Fig. 4J). In conclusion, ATO-treated AML cells activate the Caspase-3-GSDME pathway, inducing pyroptosis and releasing HMGB1 and other DAMPs. The released DAMPs further activate NKs to release GZMB, thereby triggering the ICD mechanism and promoting tumor cell death (Fig. 4K).

ATO is well-established in the clinical chemotherapy of leukemia and is recognized for its ability to directly target and kill AML cells. However, the clinical application of ATO treatment has shown unsatisfactory outcomes [27]. Further mechanisms underlying ATO treatment need to be explored. In this study, we demonstrate that ATO induces pyroptosis *via* the GSDME pathway, and that pyroptosis triggers the release of DAMPs, particularly HMGB1, thereby further inducing ICD, which promotes recruitment of NKs and the release of GZMB and contributes to the coordinated killing of tumor cells. This discovery not only offers new insights into the therapeutic mechanisms of ATO but also proposes novel strategies for treating drug-resistant recurrent tumors.

By analyzing published datasets of AML patients, we found that pyroptosis plays a key role in AML prognosis and ATO treatment outcomes (Fig. S1). This led us to hypothesize that pyroptosis may play a pivotal role in ATO treatment. We then conducted cell experiments, during which we observed that AML cells treated with ATO exhibited typical pyroptotic morphology in a dose-dependent manner (Fig. 1A), which is a key feature of pyroptotic cells. A previous studies have shown that activated caspase-3 (cleaved-caspase-3) cleaves GSDME-FL at its central linker, liberating the GSDME-N to form pores in the plasma membrane, leading to pyroptosis. Consistently, further mechanistic investigations *in vitro* and *in vivo* demonstrate that ATO induces pyroptosis *via* the CASP-GSDME pathway (Figs. 1B and 2E), and that this pyroptosis can be mitigated by pyroptosis inhibitors (Figs. 1F and G). Furthermore, GSDME-N can stimulate the expression of NLRP3, an inflammasome that facilitates the maturation and release of IL-1β [28]. Our results also demonstrate that GSDME-N upregulates the expression of NLRP3 (Figs. 2E and 3C), and thus enhances the release of the pro-inflammatory cytokine IL-1β *in vivo* (Figs. 2G and 3D). In summary, ATO treatment induces pyroptosis *via* the CASP-GSDME pathway.

Activation of gasdermins not only permits the release of pro-inflammatory cytokines but also facilitates the release of DAMPs, which can activate anti-tumor immune responses and elicit long-term efficacy of chemotherapeutic drugs [29]. Thus, we investigated the DAMPs released by ATO-induced pyroptotic cells through proteomic analysis and found that ATO stimulated AML cells to release immune-related proteins, specifically HMGB1 (Fig. S2). HMGB1 is one of the most critical DAMPs associated with pyroptosis and plays a crucial role in stimulating immune responses [30]. We identified that ATO-induced pyroptosis stimulated the extracellular release of HMGB1 (Figs. S2D–E). Our experiments also demonstrated that ATO-induced release of HMGB1 was observed *in vivo* (Fig. 2H), and this phenomenon was abolished when GSDME was knocked out (Fig. 3F). These findings indicate that ATO-induced pyroptosis promotes the release of HMGB1. However, HMGB1 levels exhibited no significant changes in GSDME-knockdown models, potentially attributed to compensatory regulatory pathways, such as nuclear factor-κB (NF-κB) signaling and microRNA-mediated mechanisms, that maintain its basal expression [31]. Notably, the progression of AML following GSDME knockdown was associated with enhanced HMGB1 release triggered by cellular stress responses, which may serve as a compensatory mechanism to offset the functional loss of GSDME.

Furthermore, previous studies have shown that HMGB1 functions to recruit inflammatory cells and mediate signaling between NKs and other immune cells [32–35]. Therefore, we focused on whether ATO-induced pyroptosis could further trigger the occurrence of the ICD mechanism. To further investigate the mechanism underlying the anti-leukemia activity of ATO treatment *in vivo*, we performed label-free quantitative proteomic analysis to identify DEPs in AML xenograft tumors. Consistent with our hypothesis, KEGG pathway analysis suggests that ATO treatment primarily mobilizes the immune system in AML xenograft mice (Figs. S3A–D). Next, we assessed the activity of NKs *in vivo*. The results show that ATO treatment significantly increased the activation and infiltration of NKs, along with enhanced GZMB release (Figs. 4A and C–E). This activation and release were notably rescued after GSDME knockdown (Figs. 4B and F). Additionally, *in vitro* co-culture experiments confirmed that ATO activates NKs to release GZMB *via* the pyroptosis pathway (Figs. 4G–J). In summary, ATO-induced pyroptosis enhances the release of DAMPs (HMGB1) and pro-inflammatory cytokines, which in turn promotes the recruitment and tumor infiltration of NKs, leading to increased GZMB expression and release in the microenvironment, thereby further contributing to tumor cell destruction.

Furthermore, both the MAPK and NOD-like receptor signaling pathways were activated in the proteomic analysis (Fig. S3E). Previous studies have shown that these two signaling pathways are crucial for the initiation of pyroptosis and the induction of cancer

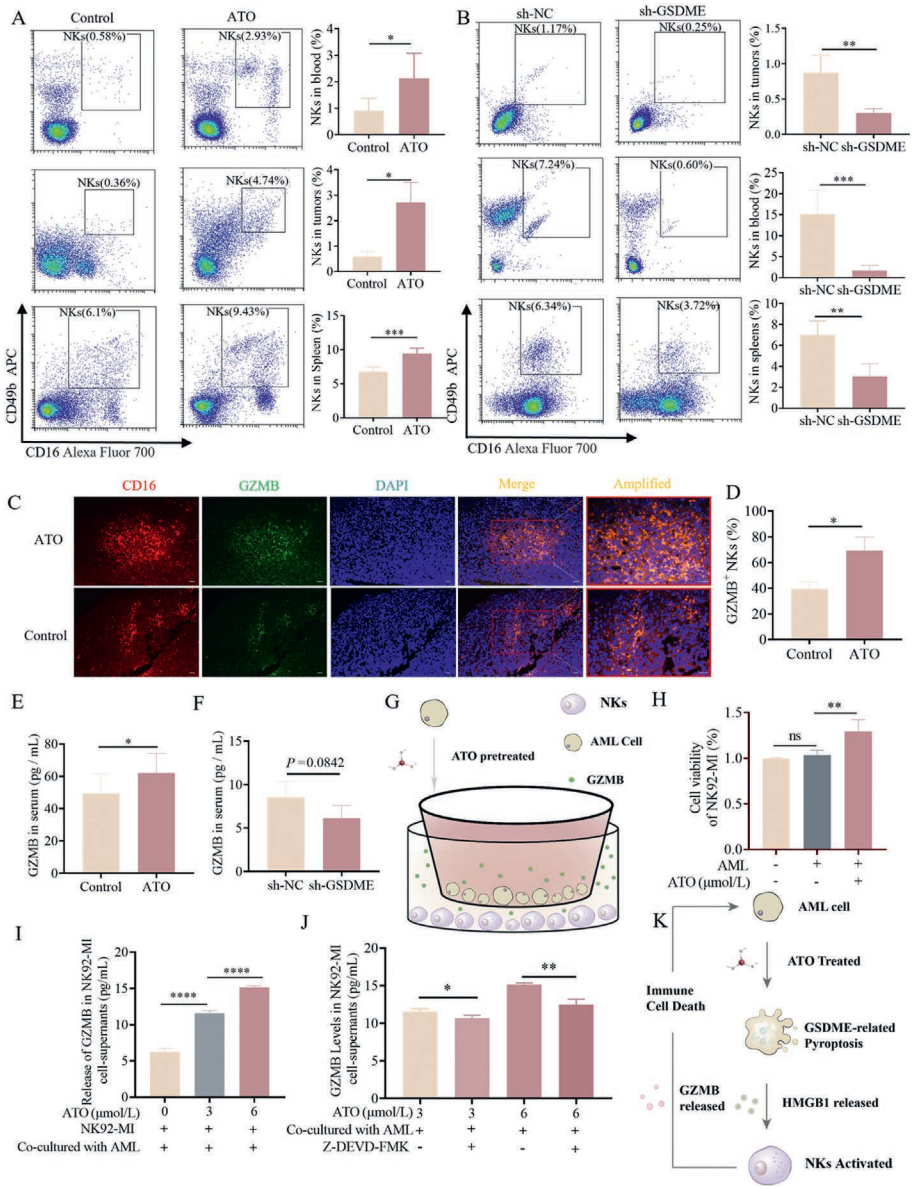


Fig. 4. Pyroptosis induced by ATO stimulates the recruitment and GZMB release of NKs *in vivo*. (A, B) NKs in the blood, tumor and spleen were stained with anti-mouse CD49b-APC and anti-mouse CD16-AF700 antibodies, followed by flow cytometric analysis. (A) Data from NC and 3 mg/kg ATO-treated xenograft mice, and (B) data from the sh-GSDME and sh-NC groups after 3 mg/kg ATO treatment. (C, D) Representative images of immunofluorescence staining of AML xenograft tumors in the ATO group and the control group, indicating co-localization of CD16 (red) with GZMB (green). Cell nuclei were counterstained with 4′,6-diamidino-2-phenylindole (DAPI) (blue). Scale bar: 50 μm. (E, F) The release levels of GZMB in the serum of AML xenograft mice were quantified by ELISA in different groups. (G) Schematic representation of the *in vitro* co-culture model. (H) Assessment of cell viability in NK92-MI cells in the control and co-culture groups. (I, J) The release levels of granzyme B (GZMB) in the supernatants of NK92-MI cells were quantified by ELISA. Z-DEVD-FMK (25 μmol/L), a caspase-3 specific inhibitor, was included in the reaction to inhibit caspase-3 activity. (K) Schematic diagram of pyroptosis induced NK-related ICD mechanism. All data are presented as mean ± SD from at least 3 independent experiments. $^{*}P < 0.05$, $^{**}P < 0.01$, $^{***}P < 0.001$, $^{****}P < 0.0001$ using two-way ANOVA test.

cell death [36–38]. The DEPs in these pathways included p38, p53, CTSB, and NLRP3, all of which showed upregulation in our study (Fig. S3). As previously reported, p53 can be uniquely activated by HMGB1 and p38 [39,40], and in turn, p53 promotes GSDME transcription [38], which may convert apoptosis into pyroptosis [41]. Here, we demonstrated that ATO upregulates the expression of p38 and p53, as well as the release of HMGB1, which may contribute to the induction of pyroptosis. Moreover, DAMPs (HMGB1 and LDH) released from pyroptotic cells can induce lysosome destabilization and stimulate the release of CTSB [42], which in turn can directly activate the NLRP3 inflammasome, leading to the maturation and release of IL-1β [43]. Our results show that ATO-induced pyroptosis enhances the expression of NLRP3 and CTSB in AML xenograft tumors, simultaneously increasing the release of HMGB1, LDH, and IL-1β.

Nevertheless, there are some limitations in this research. Regarding the mechanism of ATO-induced pyroptosis, our study focused only on the caspase-3/GSDME pathway, while recent studies have shown that GZMB can directly cleave GSDME. It remains to be investigated whether ATO-induced pyroptosis could be regulated by a positive feedback loop involving the GZMB/GSDME pathway in AML. We plan to expand our research in the future to gain a more comprehensive understanding of the effects of ATO on AML.

In conclusion, our findings indicate that ATO induces pyroptosis in AML cells *via* the caspase-3/GSDME pathway, leading to the release of HMGB1 and the pro-inflammatory cytokine IL-1β.

Additionally, we show that ATO-induced pyroptosis activates the ICD mechanism, which enhances the recruitment and infiltration of NKs within the AML microenvironment. This study sheds light on the mechanisms how ATO exerts its anti-tumor effects, providing valuable insights into its potential applications in immunotherapy and combination treatments, and suggesting potential therapeutic strategies for patients with relapsed and drug-resistant tumors.

Declaration of competing interest

The authors declare that they have no known competing financial interests or personal relationships that could have appeared to influence the work reported in this paper.

CRediT authorship contribution statement

Jia-Yin Su: Writing – original draft, Validation, Project administration, Methodology, Investigation. **Shiyao Song:** Writing – original draft, Validation, Project administration, Methodology, Investigation. **Zi-Min Song:** Writing – original draft, Project administration, Methodology, Investigation. **Xi Sun:** Validation, Software, Resources. **Niangji Tsomo:** Visualization, Software, Resources. **Ying-Li Liu:** Visualization, Validation, Software. **Jingxuan Ma:** Validation, Software, Resources. **Jie-Si Luo:** Visualization, Validation, Resources. **Li-Na Wang:** Project administration. **Suoyu Xiang:** Methodology, Investigation. **Cong Liang:** Visualization, Validation. **Xue-Qun Luo:** Validation, Software. **Jun Wu:** Writing – review & editing, Supervision, Conceptualization. **Li-Bin Huang:** Writing – review & editing, Supervision, Funding acquisition, Conceptualization. **Yan-Lai Tang:** Writing – review & editing, Supervision, Funding acquisition, Conceptualization.

Acknowledgments

This study was financially supported by grants from the Guangdong Basic and Applied Basic Research Foundation (Nos. 2023A1515030060, 2020A1515010282), the Science and Technology Planning Project of Guangdong Province (Nos. 2021A0505060004, A2021352), the Scientific Research Project of Guangdong Traditional Chinese Medicine (No. A20201056), and the Youth Talent Support Program of Guangdong Provincial Association for Science and Technology (No. SKXRC202316).

Supplementary materials

Supplementary material associated with this article can be found, in the online version, at doi:10.1016/j.cclet.2025.111585.

References

[1] E. Lengfelder, W.K. Hofmann, D. Nowak, Leukemia 26 (2012) 433–442.
[2] F. LoCoco, G. Avvisati, M. Vignetti, et al., N. Engl. J. Med. 369 (2013) 111–121.
[3] J.S. Luo, X.L. Zhang, D.P. Huang, et al., Ann. Hematol. 102 (2023) 1713–1721.
[4] D.P. Huang, L.C. Yang, Y.Q. Chen, et al., Blood Cancer J. 13 (2023) 178.
[5] C.J. Peng, Z. Fan, J.S. Luo, et al., Technol. Cancer Res. Treat. 23 (2024) 15330338231223080.
[6] M. Sonksen, K. Kerl, H. Bunzen, Med. Res. Rev. 42 (2022) 374–398.
[7] X. Li, Y.F. Pan, Y.B. Chen, et al., Cell Death Dis. 15 (2024) 300.
[8] K. Moloudi, A. Neshasteriz, A. Hosseini, et al., Iran Biomed. J. 21 (2017) 330–337.
[9] P.R. Subbarayan, B. Ardalan, J, Gastrointest. Cancer 45 (2014) 363–371.
[10] J. Shi, Y. Zhao, K. Wang, et al., Nature 526 (2015) 660–665.
[11] J. Gao, X. Zhang, K. Shang, et al., Chin. Chem. Lett. 31 (2020) 427–430.
[12] S.M. Man, R. Karki, T.D. Kanneganti, Immunol. Rev. 277 (2017) 61–75.
[13] J. Ding, K. Wang, W. Liu, et al., Nature 535 (2016) 111–116.
[14] J. Shi, W. Gao, F. Shao, Trends Biochem. Sci. 42 (2017) 245–254.
[15] G. Zhong, F. Wan, J. Lan, et al., Sci. Total Environ. 788 (2021) 147780.
[16] L.L. Zhang, D.J. Zhang, J.X. Shi, et al., Phytomedicine 132 (2024) 155828.
[17] A.D. Garg, P. Agostinis, Immunol. Rev. 280 (2017) 126–148.
[18] J. Wen, X. Zhang, Front. Biosci. 28 (2023) 260.
[19] Y. Gao, R. Zhou, Q. Wang, et al., Chin. Chem. Lett. 35 (2024) 109521.
[20] F. Shao, Nat. Rev. Immunol. 21 (2021) 620–621.
[21] A. Coppola, B. Capuani, F. Pacifici, et al., Int. J. Mol. Sci. 22 (2021) 7988.
[22] G. Bossi, G.M. Griffiths, Nat. Med. 5 (1999) 90–96.
[23] Z. Zhang, Y. Zhang, S. Xia, et al., Nature 579 (2020) 415–420.
[24] Z. Zhou, H. He, K. Wang, et al., Science 368 (2020) 6494.
[25] T. Hoegen, N. Tremel, M. Klein, et al., J. Immunol. 187 (2011) 5440–5451.
[26] B. Zhou, D.W. Abbott, Cell Rep. 35 (2021) 108998.
[27] H.H. Zhu, Y.Z. Qin, Z.L. Zhang, et al., Blood Adv. 7 (2023) 2972–2982.
[28] B.L. MundyBosse, S.D. Scoville, L. Chen, et al., J. Clin. Invest. 126 (2016) 4404–4416.
[29] A. Ahmed, S.W.G. Tait, Mol. Oncol. 14 (2020) 2994–3006.
[30] D.V. Krysko, A.D. Garg, A. Kaczmarek, et al., Nat. Rev. Cancer 12 (2012) 860–875.
[31] Y. Cui, X. Wu, J. Jin, et al., Mol. Cancer 22 (2023) 179.
[32] M.T. Lotze, K.J. Tracey, Nat. Rev. Immunol. 5 (2005) 331–342.
[33] A. Murao, M. Aziz, H. Wang, M. Brenner, P. Wang, Apoptosis 26 (2021) 152–162.
[34] M. Lamkanfi, A. Sarkar, L. Vande Walle, et al., J. Immunol. 185 (2010) 4385–4392.
[35] L. Hou, Z. Yang, Z. Wang, et al., Lab. Invest. 98 (2018) 1052–1064.
[36] Y. Masuda, M. Futamura, H. Kamino, et al., J. Hum. Genet. 51 (2006) 652–664.
[37] M.B. Düzgün, K. Theofilatos, A.G. Georgakilas, A. Pavlopoulou, Oxid. Med. Cell Longev. 2019 (2019) 4606219.
[38] L. Jayaraman, N.C. Moorthy, K.G. Murthy, et al., Genes Dev. 12 (1998) 462–472.
[39] W.O. Chae, G.D. Kim, J. Cancer Prev. 26 (2021) 183–194.
[40] H. Lin, Y. Wang, H. Lai, X. Li, T. Chen, Chem. Asian J. 13 (2018) 2730–2738.
[41] C. Rogers, T. FernandesAlnemri, L. Mayes, et al., Nat. Commun. 8 (2017) 14128.
[42] S. Kumar, M. Dhiman, Microb. Pathog. 125 (2018) 468–474.
[43] A. Chevriaux, T. Pilot, V. Derangère, et al., Front. Cell Dev. Biol. 8 (2020) 167.